International Journal of Solids and Structures 49 (2012) 514–526

Contents lists available at SciVerse ScienceDirect

International Journal of Solids and Structures

journal homepage: www.elsevier.com/locate/ijsolstr

Nonlinear vibrations and instabilities of a stretched hyperelastic annular membrane

Renata M. Soares [a], Paulo B. Gonçalves [b,*]

[a] School of Civil Engineering, Federal University of Goiás, UFG 74605-200, Goiânia, GO, Brazil
[b] Civil Engineering Department, Pontifical Catholic University, PUC-Rio, 22451-900 Rio de Janeiro, RJ, Brazil

ARTICLE INFO

Article history:
Received 15 June 2011
Received in revised form 6 September 2011
Available online 25 October 2011

Keywords:
Annular membrane
Hyperelastic material
Nonlinear vibrations
Finite deformations
Nonlinear dynamics

ABSTRACT

The mathematical modeling for the nonlinear vibration analysis of a pre-stretched hyperelastic annular membrane under finite deformations is presented. The membrane is initially fixed along the inner boundary and then subjected to a uniform radial traction along its outer circumference and fixed along the outer boundary. The pre-stretched membrane in then subjected to a transversal harmonic pressure. The membrane material is assumed to be homogeneous, isotropic, and neo-Hookean. First, the solution of the radially stretched membrane is obtained analytically and numerically by the shooting method. The equations of motion of the stretched membrane are then obtained. By analytically and numerically solving the linearized equations of motion, the vibration modes and frequencies of the hyperelastic membrane are obtained, and these normal modes are used, together with the Galerkin method, to obtain reduced order models for the nonlinear dynamic analysis. A parametric analysis of the nonlinear frequency-amplitude relations, resonance curves, bifurcation diagrams and basins of attraction show the influence of the initial stretching ratio and membrane geometry on the type and degree of nonlinearity of the hyperelastic membrane under large amplitude vibrations. To check the accuracy of the reduced order models and the influence of the simplifying hypotheses on the results, the same problem is also analyzed using the finite element method. Excellent agreement is observed.

1. Introduction

Membranes have received considerable attention in recent years due to their use in numerous engineering areas, including space applications, actuators, sensors, robotics, bioengineering, biology, aero-space industry and civil engineering structures. A review of the literature on the static and dynamic behavior of membranes, with emphasis in practical applications, can be found in Jenkins and Leonard (1991) and Jenkins and Korde (2006).

The analysis of membranes is an important research topic in nonlinear continuum mechanics. In particular, the study of hyperelastic membranes under finite deformations, such as elastomeric membranes and most biological tissues, is a rather challenging subject, and, in such cases, elasticity in the fully nonlinear range must be employed. The pioneering works of Rivlin (1948a,b) on nonlinear elasticity is the basis for the analysis of structures under large deformations. The first developments in this field are collected in the classical work by Green and Adkins (1960). Recent advances in finite elasticity and useful historical reviews can be found in Libai and Simmonds (1998) and Fu and Ogden (2001). The reader may refer to the works by Selvadurai (2006) and Saccomandi and Ogden (2004) for critical reviews on constitutive models for hyperelastic materials.

In a previous paper the authors studied the linear and nonlinear vibrations of a circular hyperelastic membrane using different constitutive laws with emphasis on some important nonlinear characteristics, such as frequency-amplitude relation, resonance curves, bifurcations and dynamic integrity (Gonçalves et al., 2009). In the present paper the analysis of a pre-stretched annular membrane is conducted.

The static linear and nonlinear analysis of annular membranes under various loading conditions and subjected to small and large deformation has been conducted by several researchers in the past. Na and Kurajian (1976) analyzed the displacements and stresses of annular membranes under pressure transforming the nonlinear boundary value problem into an initial value problem. Hite and Peddieson (1977) analyzed numerically the moderate to large axisymmetric displacements of annular membranes with the aid of Foppl's equations. Solutions by finite difference method were obtained for different sets of boundary conditions. Fulton and Simmonds (1986) studied an initially flat annular membrane subjected to symmetric transversal loads along the boundaries. Deformation and load–displacement curves are obtained for membranes fixed at its outer edge and attached to a rigid inclusion in the inner edge. Four strain energy densities are considered:

* Corresponding author Address: Department of Civil Engineering, PUC-Rio Rua Marquês de São Vicente, 225, Gávea 22451-900 Rio de Janeiro, RJ, Brazil. Tel.: +55 21 3527 1188; fax: +55 21 3527 1195.
E-mail address: paulo@puc-rio.br (P.B. Gonçalves).

0020-7683/$ - see front matter © 2011 Elsevier Ltd. All rights reserved.
doi:10.1016/j.ijsolstr.2011.10.019

classical, neo-Hookean, Mooney–Rivlin and Saunders. For a point load, it is observed that the displacement, when the material is a classic, neo-Hookean or Mooney material, is infinite and when the material is considered to be of the Rivlin–Saunders type the displacement is finite to a certain range of parameters. Grabmüller and Novak (1987) studied the axisymmetric deformations of annular membranes under uniform distributed loading normal to its surface using Föppl's deformation theory. Tezduyar et al. (1987) analyzed the static transverse deformations caused by a rigid body attached to the center of an annular membrane made of a Mooney–Rivlin isotropic and incompressible material. Experimental and numerical investigation of the large deflections of an annular membrane subjected to transversal edge loads and torsion was conducted by Pamplona and Bevilacqua (1992) while the stability and wrinkling of the membrane described by the Mooney–Rivlin constitutive model under torsion was studied by Roxburgh et al. (1995). Redistribution of the stresses due to a circular hole in a nonlinear anisotropic membrane, a problem found in many clinical procedures, was investigated by David and Humphrey (2004). The large elastic deformations of a prestretched right circular annular cylinder was studied recently by Saravanan (2011).

The linear vibration analysis of homogeneous elastic annular membrane is a classical problem in mechanics and in the theory of partial differential equations, where this problem is modeled by a bi-dimensional wave equation in polar coordinates (Asmar, 2005). Several aspects of this problem have been analyzed in the past (Laura et al., 1998; Gutierrez et al., 1998 and Buchanan, 2005). The natural frequencies and vibration modes of circular and annular membranes with a varying density along the radial direction were studied by Jabareen and Eisenberger (2001), Bala Subrahmanyam and Sujith (2001) and Willatzen (2002). Later, the linear dynamic behavior of an annular membrane with a rigid inclusion was examined by Wang (2003). An analytical and experimental investigation on a vibrating annular membrane attached to a central, rigid core was conducted by Pinto (2006). Noga (2010) studied the linear free transversal vibrations of a system of two annular and circular membranes connected by a Winkler elastic layer using analytical methods and numerical simulation. The works by Jiang (1996), Chakravarty and Albertani (2010) and Chang-Jiang et al. (2010), among others, shed some light on the nonlinear vibrations of membrane structures. Wang and Steigmann (1997) studied the small oscillations of finitely deformed elastic networks considering a non-uniform underlying equilibrium state of the membrane in the modal analysis of the linearized equations.

However little is known on the linear and particularly nonlinear vibrations of hyperelastic membranes. Zhu et al. (2010) studied the resonant behavior of a prestretched membrane of a dielectric elastomer using the large deflection membrane theory. This problem had been previously analyzed by Goulbourne et al. (2004, 2005) and Fox and Goulbourne (2008, 2009). Recently, Zhu et al. (2010) also analyzed the nonlinear oscillations of an elastomeric balloon.

The aim of this work is to conduct a detailed parametric analysis of the linear and nonlinear free and forced vibrations of an annular hyperelastic membrane. The mathematical modeling for the nonlinear vibration analysis of a pre-stretched hyperelastic annular membrane under finite deformations is presented. The membrane is initially fixed along the inner boundary and then subjected to a uniform radial traction along its outer circumference, then fixed along the outer boundary and subjected to a transversal harmonic pressure. The membrane material is assumed to be homogeneous, isotropic, and neo-Hookean. First, the solution of the stretched membrane is obtained analytically and numerically. The results shows that the solution is a function of the material constant, the stretching ratio in the radial direction (deformed external radius/ undeformed external radius) and the ratio of the inner to the outer radius. The equations of motion of the stretched membrane are then obtained. By analytically and numerically solving the linearized equations of motion, the vibration modes and frequencies of the hyperelastic membrane are obtained, and these normal modes are used, together with the Galerkin method, to obtain reduced order approximations of the nonlinear dynamic response. The same problem is also analyzed using the finite element software Abaqus® (Abaqus, 2001). The development of low order models in nonlinear dynamics enables the efficient use of several numerical algorithms and geometric tools, being in recent years an important research area (Rega and Troger, 2005 and Nayfeh and Balashandran, 1995). The results show that a model with a small number of degrees of freedom can give accurate results up to very large deflections. The accuracy of this low order model is verified via comparisons with the higher order modal approximations, and the numerical values computed by the finite element method, which compare well with the theoretical results. The results highlight the influence of the stretching ratio and annular membrane geometry on the vibration frequencies, nonlinear frequency-amplitude relation, and bifurcation diagrams.

The knowledge of the large deformations and vibration characteristics of annular and circular membranes is of importance in many practical applications, including musical instruments (Rossing, 2000) and microphone diaphragms (Lavergne et al., 2010; Pinto, 2006). Also there are many biomedical problems where the knowledge of the annular membrane vibrations is important. These include the problem of tympanic membrane perforation and related surgical procedures as the insertion of grafts or ventilation tubes (Prendergast et al., 1999; Tobis et al., 2009; Volandri et al., 2011) and ophthalmology (David, 2005). In addition polymeric hyperelastic membranes such as expanded membranes have been used in some surgical procedures (Lladó et al., 1999). In the field of biology, for example sound production systems and modification of vibrations in various animals (animal resonators) is based on forced flow through an orifice and/or past a thin membrane (Decraemer et al., 1989; Recio et al., 1998). Another interesting problem involving the large deformations of annular membrane is in the field of cell mechanobiology (Balestrini et al., 2010). Also, in recent years, intensive research has been conducted on the development of new membrane materials, including shape memory polymers and dielectric elastomers, which are of interest for use in sensors and vibration control, bioengineering and thin-films used in compliant micro devices (Pelrine et al., 2000; Goulbourne et al., 2004, 2005; Fox and Goulbourne, 2008, 2009; Zhu et al., 2010).

2. Theoretical framework

Consider an undeformed homogeneous, isotropic hyperelastic circular membrane of thickness h and mass per unit area Γ with an outer radius R_e and having a central hole of radius R_o. The membrane is initially fixed along the inner circular boundary and then subjected to a uniform radial traction along its outer circumference, reaching a deformed external radius R_f. The stretched membrane is then fixed along the outer boundary and subjected to a time-dependent lateral pressure $p(\rho,\theta,t)$.

The mechanical behavior of many rubber-like materials can be described via the neo-Hookean energy density function (Foster, 1967b; Wong and Shield, 1969; Treloar, 1975; Chou-Wang and Horgan, 1989; Wineman, 2005).

$$W = C_1(I_1 - 3) \tag{1}$$

where C_1 is an empirically determined material constant and I_1 is the first invariant of the deformation tensor, which can be written in terms of the principal stretches as

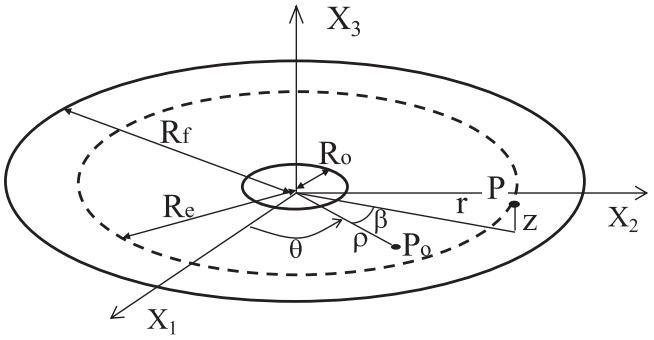

Fig. 1. Undeformed and deformed configurations: geometry and coordinate systems.

$$I_1 = J^{-2/3}\bar{I}_1; \quad \bar{I}_1 = \lambda_1^2 + \lambda_2^2 + \lambda_3^2 \tag{2}$$

where, for an incompressible material, $J = \lambda_1\lambda_2\lambda_3 = 1$.

The deformed and undeformed geometry are shown in Fig. 1. Using the usual cylindrical coordinate system, the position of a material point P_o on the undeformed mid-surface reference plane originally at $(\rho,\theta,0)$ is mapped into a deformed position P defined by the quantities r, β and z, as shown in Fig. 1, following the application of the loads. The coordinates of point P_o, in a coordinate system with the origin at the center of the annular membrane, are given by:

$$\begin{aligned} X_1 &= \rho\cos\theta \\ X_2 &= \rho\sin\theta \\ X_3 &= 0 \end{aligned} \tag{3}$$

where ρ and θ are the radial and circumferential coordinates, respectively.

The coordinates of the same point P, at a given instant t, in a deformed configuration, are given by:

$$\begin{aligned} x_1 &= r(\rho,\theta,t)\cos\beta(\rho,\theta,t) \\ x_2 &= r(\rho,\theta,t)\sin\beta(\rho,\theta,t) \\ x_3 &= z(\rho,\theta,t) \end{aligned} \tag{4}$$

where r, β, and z are the radial, circumferential, and transversal coordinates of the deformed membrane, respectively. The polar coordinates ρ and θ and time t are taken as independent variables.

The displacement field can be written as the sum of the axisymmetric field due to the uniform radial pre-stress state plus a dynamic field due to the applied time-dependent load, that is

$$\begin{aligned} r(\rho,\theta,t) &= r_o(\rho,\theta) + u(\rho,\theta,t) \\ \beta(\rho,\theta,t) &= \theta + v(\rho,\theta,t) \\ z(\rho,\theta,t) &= w(\rho,\theta,t) \end{aligned} \tag{5}$$

where $w(\rho,\theta,t)$, $u(\rho,\theta,t)$ and $v(\rho,\theta,t)$ are the perturbation components in the radial, transversal and circumferential directions, respectively, and $r_o(\rho,\theta)$ describes the initial deformed static state.

Defining the principal strains as $\lambda_i = dS_i/ds_i$, where dS_i and ds_i, are the deformed and undeformed lengths, respectively, of an infinitesimal element in the principal directions, the following expressions are obtained for in-plane principal strains:

$$\lambda_1 = \sqrt{r_{,\rho}^2 + r^2\beta_{,\rho}^2 + z_{,\rho}^2} \tag{6}$$

$$\lambda_2 = \sqrt{r_{,\theta}^2 + r^2\beta_{,\theta}^2 + z_{,\theta}^2} \tag{7}$$

where $\partial(\,)/\partial\rho = (\,)_{,\rho}$ and $\partial(\,)/\partial\theta = (\,)_{,\theta}$.

Taking into account the incompressibility condition, the principal strain in the normal direction is $\lambda_3 = 1/\lambda_1\lambda_2$, or, physically, $\lambda_3 = H/h$, where H is the deformed membrane thickness. This term generates the nonlinear terms in the equations of motion.

Thus, the first invariant I_1 is given by:

$$\begin{aligned} I_1 &= \sum_{i=1}^{3}\lambda_i^2 \\ &= r_{,\rho}^2 + r^2\beta_{,\rho}^2 + z_{,\rho}^2 + \frac{r_{,\theta}^2 + r^2\beta_{,\theta}^2 + z_{,\theta}^2}{\rho^2} \\ &\quad + \frac{\rho^2}{(r_{,\rho}^2 + r^2\beta_{,\rho}^2 + z_{,\rho}^2)(r_{,\theta}^2 + r^2\beta_{,\theta}^2 + z_{,\theta}^2) - (r_{,\rho}r_{,\theta} + r^2\beta_{,\rho}\beta_{,\theta} + z_{,\rho}z_{,\theta})^2} \end{aligned} \tag{8}$$

The elastic strain energy U is the volume integral of W in the undeformed configuration, which in the present case becomes:

$$U = \int_{R_o}^{R_e}\int_0^{2\pi}\int_0^{h}\rho W(\rho, r, r_{,\rho}, r_{,\theta}, z_{,\rho}, z_{,\theta}, \beta_{,\rho}, \beta_{,\theta}, \rho, \theta)\,dz\,d\theta\,d\rho \tag{9}$$

The work term W_e, considering a radial stretch due to a uniform distributed force f along the circular boundary, and a uniform pressure $p_h(t)$, is (Tielking and Feng, 1974):

$$W_e = 2\pi\rho f(r_o - \rho)|_{\rho=R_e} + p_h(t)\Delta V \tag{10}$$

where $\Delta V = V_f - V_0$ is the variation of the volume enclosed by the structure due to the pressure, V_f is the volume enclosed by the deformed membrane, and $V_0 = 0$ is the volume enclosed by the undeformed, initially flat, membrane.

The kinetic energy is written as:

$$T = \int_{R_o}^{R_e}\int_0^{2\pi}\int_0^{h}\Gamma\frac{(\dot{r}^2 + \dot{\beta}^2 + \dot{z}^2)}{2}\rho\,dz\,d\theta\,d\rho \tag{11}$$

where $\dot{(\,)} = \partial(\,)/\partial t$.

3. Static analysis

For the membrane under uniform radial traction the principal strains reduces to

$$\lambda_1 = \frac{dr_o}{d\rho} \quad \lambda_2 = \frac{r_o}{\rho} \quad \lambda_3 = \frac{\rho}{r_o r_{o,\rho}} \tag{12}$$

and the first invariant I_1 to:

$$I_1 = r_{o,\rho}^2 + \frac{r_o^2}{\rho^2} + \frac{\rho^2}{r_o^2 r_{o,\rho}^2} \tag{13}$$

So, the strain energy of the neo-Hookean membrane is given by:

$$U = \int_{R_o}^{R_e}\int_0^{2\pi} C_1 h\left[r_{o,\rho}^2 + \frac{r_o^2}{\rho^2} + \frac{\rho^2}{r_o^2 r_{o,\rho}^2} - 3\right]\rho\,d\theta\,d\rho \tag{14}$$

Using the stationary energy principle, the equilibrium equation in the radial direction is obtained:

$$\frac{r_o}{\rho} - \frac{3\rho^3}{r_o^3(r_{o,\rho})^2} - r_{o,\rho} + \frac{3\rho^2}{r_o^2(r_{o,\rho})^3} - \left(\frac{3\rho^3}{r_o^2(r_{o,\rho})^4} + \rho\right)r_{o,\rho\rho} = 0 \tag{15}$$

Two boundary conditions are necessary to obtain the solution of the boundary value problem. In the inner edge, $r_o(R_o) = R_o$. In the outer edge, the boundary condition can be written in terms of the traction force per unit boundary length, f, or as an imposed displacement, that is:

$$f = \frac{2hC_1}{R_e r_o^2 r_{o,\rho}^3}\left(r_o^2(r_{o,\rho})^4\rho - \rho^3\right); \quad \text{or} \quad r_o(R_e) = R_f \tag{16}$$

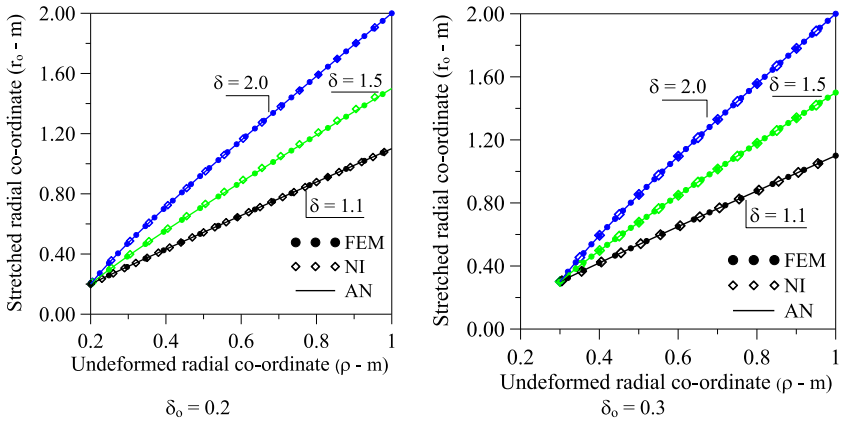

Fig. 2. Variation of the deformed radius for selected values of the stretching ratio δ. FEM: finite element method, NI: numerical integration, AN: analytical results (Eq. (21)).

The nonlinear Eq. (15) is converted into a system of first-order differential equations

$$y(\rho) = \frac{dr_o}{d\rho} \tag{17.a}$$

$$\frac{dy(\rho)}{d\rho} = -\left(\frac{r_o^4(r_{o,\rho})^4 - 3\rho^4 r_{o,\rho} - \rho r_o^3(r_{o,\rho})^5 + 3\rho^3 r_o^3 r_{o,\rho}}{\rho^2 r_o(3\rho^2 + r_o^2(r_{o,\rho})^4)}\right) \tag{17.b}$$

and solved numerically by the shooting method, which converts the boundary value problem into an initial value problem. Being the inner radius prescribed, $r_o(R_o) = R_o$, the derivative $r_{o,\rho}(R_o)$ is varied until the boundary condition $r_o(R_e) = R_f$ is satisfied within a desired tolerance. The first order differential equations are integrated by the Runge–Kutta method and convergence of the initial condition $r_{o,\rho}(R_o)$ is achieved by the use of the Newton–Raphson method.

In Soares (2009), the displacement field obtained through the numerical integration is approximated, as:

$$r_o(\rho) = A_1 \log(\rho) + A_2\rho^2 \log\rho + A_3\rho^2 + A_4\rho + A_5 \tag{18}$$

and the coefficients A_i are determined using the least square method.

Alternatively, linearizing the equilibrium Eq. (15), the following Euler–Cauchy differential equation is obtained:

$$r_o - \rho r_{o,\rho} - \rho^2 r_{o,\rho\rho} = 0 \tag{19}$$

By applying the boundary conditions and considering the non-dimensional parameters

$$\bar{r}_o = r_o/R_e, \quad \delta = R_f/R_e, \quad \delta_o = R_o/R_e, \quad \bar{\rho} = \rho/R_e \tag{20}$$

the following analytical solution is obtained in terms of the two deformation parameters

$$\bar{r}_o(\rho) = \frac{1}{(1-\delta_o^2)}\left[(\delta-\delta_o^2)\bar{\rho} + \delta_o^2(1-\delta)\bar{\rho}^{-1}\right] \tag{21}$$

leading to the following non-dimensional stress distributions in the radial and circumferential direction, respectively

$$\bar{\sigma}_1 = 2\left\{\frac{\left[(\delta-\delta_o^2)\bar{\rho}^2 - \delta_o^2(1-\delta)\right]^2}{(1-\delta_o^2)^2}\frac{1}{\bar{\rho}^4} - \bar{\rho}^8\frac{(1-\delta_o^2)^4}{\left[(\delta-\delta_o^2)\bar{\rho}^2 + \delta_o^2(1-\delta)\right]^2\left[(\delta-\delta_o^2)\bar{\rho}^2 - \delta_o^2(1-\delta)\right]^2}\right\}$$

$$\bar{\sigma}_2 = 2\left\{\frac{\left[(\delta-\delta_o^2)\bar{\rho}^2 + \delta_o^2(1-\delta)\right]^2}{(1-\delta_o^2)^2}\frac{1}{\bar{\rho}^4} - \bar{\rho}^8\frac{(1-\delta_o^2)^4}{\left[(\delta-\delta_o^2)\bar{\rho}^2 + \delta_o^2(1-\delta)\right]^2\left[(\delta-\delta_o^2)\bar{\rho}^2 - \delta_o^2(1-\delta)\right]^2}\right\} \tag{22}$$

where $\bar{\sigma}_i = \sigma_i/C_1$ are the non-dimensional principal stresses.

An annular membrane with initial radius $R_e = 1$ m (which is equivalent to scaling all length variables by R_e), thickness $h = 0.001$ m, and mass density $\Gamma = 2200$ kg/m^3 is considered for the numerical analysis. The constant of the neo-Hookean material is $C_1 = 0.17$ MPa. The adopted stress–strain relation and material constant were obtained experimentally and are given in Selvadurai (2006) and Gonçalves et al. (2009). Two values of the internal radius, $\delta_o = 0.2$ m and $\delta_o = 0.3$ m, are adopted in the parametric analysis.

To help in the derivation of an accurate low dimensional model for the free and forced finite amplitude nonlinear vibration analysis of the membrane, the results here obtained are compared with those obtained using the finite element software Abaqus 6.5® (Abaqus, 2001).

Convergence of all static results can be obtained using the membrane elements M3D4 or M3D3 and a mesh of 9789 elements for $\delta_o = 0.2$ m and a mesh of 7070 elements for $\delta_o = 0.3$ m. The stretched configuration is accomplished by imposing an initial uniform radial displacement along the outer boundary ($R_f = \delta R_e$) in the FE program.

Fig. 2 shows the variation of the stretched radius as a function of the radial co-ordinate for three values of the stretching ratio, δ. The results obtained by numerical integration (NI) of the nonlinear equilibrium equation compare quite well with the finite element results (FEM) and those given by the analytical solution (AN), Eq. (21). The corresponding results for the principal stresses σ_1 and σ_2 are favorably compared in Fig. 3. The nonlinearity is restricted to the region close to the internal edge and increases with δ. As ρ approaches the outer edge the variation of the radial displacement and principal stresses become practically linear, with σ_1 decreasing and σ_2 increasing with ρ.

4. Dynamic analysis

Substituting (5) into the energy terms (9)–(11), the Lagrangian $L = T - U + W_e$ is obtained. By the use of Hamilton's principle, the set of three partial nonlinear equations of motion are obtained in terms of u, v and w:

$$\frac{\partial L}{\partial r} - \frac{\partial}{\partial\rho}\left(\frac{\partial L}{\partial r_{,\rho}}\right) - \frac{\partial}{\partial\theta}\left(\frac{\partial L}{\partial r_{,\theta}}\right) + \frac{\partial}{\partial t}\left(\frac{\partial L}{\partial r_{,t}}\right) = 0 \tag{23.a}$$

$$\frac{\partial L}{\partial \beta} - \frac{\partial}{\partial\rho}\left(\frac{\partial L}{\partial \beta_{,\rho}}\right) - \frac{\partial}{\partial\theta}\left(\frac{\partial L}{\partial \beta_{,\theta}}\right) + \frac{\partial}{\partial t}\left(\frac{\partial L}{\partial \beta_{,t}}\right) = 0 \tag{23.b}$$

$$\frac{\partial L}{\partial z} - \frac{\partial}{\partial\rho}\left(\frac{\partial L}{\partial z_{,\rho}}\right) - \frac{\partial}{\partial\theta}\left(\frac{\partial L}{\partial z_{,\theta}}\right) + \frac{\partial}{\partial t}\left(\frac{\partial L}{\partial z_{,t}}\right) = 0 \tag{23.c}$$

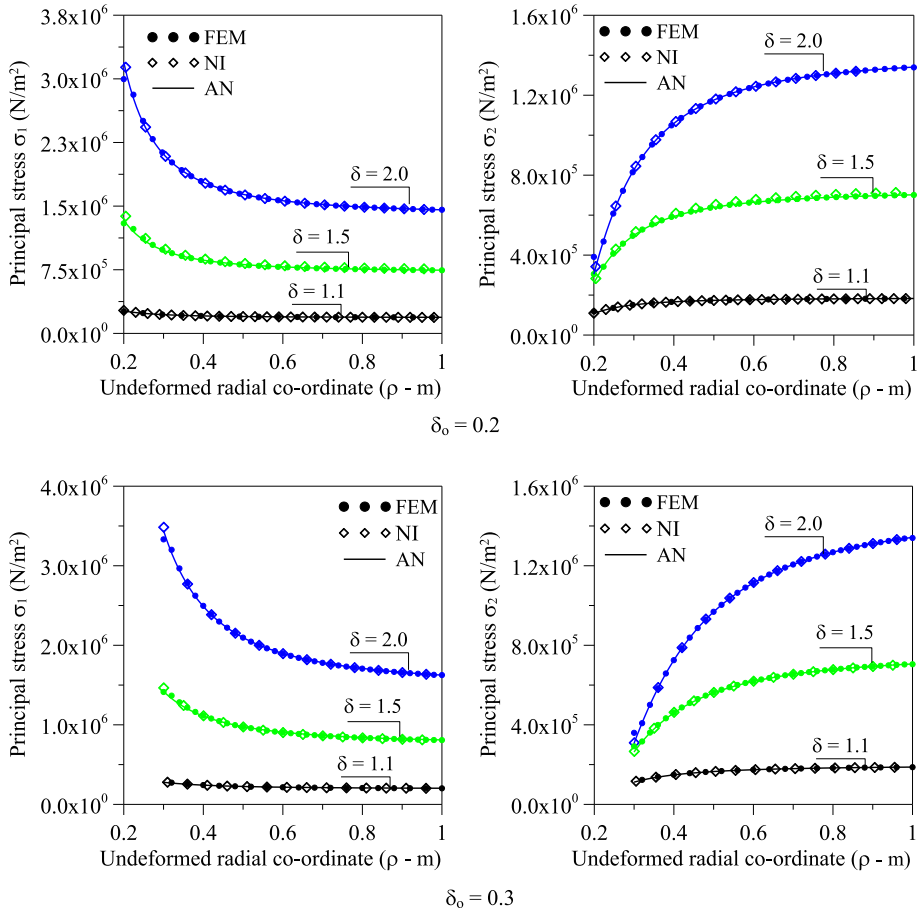

Fig. 3. Variation of the principal stresses (σ_1 and σ_2 – N/m^2) for the annular membrane, considering two values of the internal radius and three stretching ratios. FEM: finite element method, NI: numerical integration, AN: analytical results (Eq. (22)).

The uniform transversal pressure is given by:

$$P(t) = P_o \cos(\Omega t) \tag{24}$$

where *Po* is the forcing magnitude and Ω is the forcing frequency.

4.1. Linear vibration analysis

Linearizing the equation of motion in the transversal direction and substituting the solution for the deformed radius, either Eq. (18) or (21), the following equation is obtained

$$\frac{\partial^2 w(\rho,\theta,t)}{\partial t^2} = \frac{2C_1}{\Gamma}\left\{[1+L_1(\rho)]\frac{\partial^2 w(\rho,\theta,t)}{\partial \rho^2} + \left[\frac{1}{\rho}+L_2(\rho)\right]\frac{\partial w(\rho,\theta,t)}{\partial \rho} + \left[\frac{1}{\rho^2}+L_3(\rho)\right]\frac{\partial^2 w(\rho,\theta,t)}{\partial \theta^2}\right\} \tag{25}$$

where the coefficients L_i are nonlinear functions of ρ and are given in the Appendix A and B considering, respectively, Eqs. (18) and (21). The complexity of the variable coefficients precludes the derivation of closed form analytic solution for this problem.

Neglecting the coefficients L_i in (25), Eq. (25) reduces to the classical two-dimensional wave equation in polar coordinates (Asmar, 2005). For an annular membrane fixed on both boundaries the displacement $w(\rho,\theta,t)$ is given by

$$w(\rho,\theta,t) = A_{mn}\left[CJ_n\left(\frac{\Lambda_{mn}\rho}{R_e}\right) - Y_n\left(\frac{\Lambda_{mn}\rho}{R_e}\right)\right]\cos(n\theta)\cos(\omega t) \tag{26}$$

where $C = Y_n(\Lambda_{mn})/J_n(\Lambda_{mn})$, A_{mn} is the modal amplitude; J_n is the Bessel function of the first kind and order n; Y_n is the Bessel function of the second kind and order n; n is the number of waves in the circumferential direction and m denotes the m-th positive root, Λ_{mn}, of

$$W(\Lambda_{mn}) = J_n\left(\frac{R_o}{R_e}\Lambda_{mn}\right)Y_n(\Lambda_{mn}) - J_n(\Lambda_{mn})Y_n\left(\frac{R_o}{R_e}\Lambda_{mn}\right) = 0 \tag{27}$$

The solution of Eq. (25) can be accomplished by: (i) substituting a series of modal functions described by (26) into (25) and by applying the Galerkin method; or (ii) substituting (26) into (25) and retaining the relevant terms in (25). The latter procedure leads to the following approximation for the eigen frequencies (Soares, 2009):

$$\omega_{mn} = \sqrt{\frac{2\Lambda_{mn}^2 C_1}{R_e^2 \Gamma}\left(1 - \frac{1}{\delta^2 \left(r_o'(R_e)\right)^4}\right)} \tag{28}$$

where $r_o'(R_e)$ is the derivative of r_o' at $\rho = R_e$.

As δ increases, each frequency approaches from below an upper bound given by:

Table 1
Comparison of the lowest natural frequencies (rad/s).

δ	δ_o = 0.20				δ_o = 0.30			
	FEM	AN	App.1	App.2	FEM	AN	App.1	App.2
1.1	32.512	32.307	32.497	32.499	38.827	38.200	38.608	38.591
1.5	45.716	45.561	45.768	45.686	53.465	53.390	53.132	53.129
2.0	47.431	47.113	47.149	47.150	54.926	54.423	54.585	54.585

R_e = 1.0; m = 1; n = 0; natural frequencies – rad/s.

Table 2
Comparison of the natural frequencies (rad/s).

m	n	$\delta = 1.1$		$\delta = 1.5$		$\delta = 2.0$	
		AN	FEM	AN	FEM	AN	FEM
$\delta_o = 0.20$							
1	1	34.751	35.725	50.293	50.788	52.244	52.513
1	2	42.840	43.491	62.000	62.349	64.406	64.615
$\delta_o = 0.30$							
1	1	40.607	40.984	55.873	56.795	58.042	58.440
1	2	46.879	46.796	64.950	65.629	67.471	67.725

$R_e = 1.0$; natural frequencies – rad/s.

$$\omega_{nm(\delta\to\infty)} = \sqrt{\frac{2\Lambda_{nm}^2 C_1}{R_e^2 \Gamma}} \tag{29}$$

Table 1 shows the lowest natural frequencies ($m = 1; n = 0$) for selected values of δ_o and δ evaluated by: (i) the finite element method (FEM), (ii) the analytical approximation (28), and (iii) solving the Eq. (25) by the Galerkin method, considering the full variable coefficients, being these coefficients calculated by the use of (18) (Appendix A) or (21) (Appendix B). These procedures lead only to minor variations in the lowest natural frequencies, and can be considered as acceptable alternative solutions for this problem. Table 2 compare favorably the higher natural frequencies obtained by the approximate analytical solution (28) and the FE results.

Fig. 4 shows the variation of the natural frequencies with the modal wave-number m and n, considering two values of the stretching ratio δ and $\delta_o = 0.2$. The variation of ω_{mn} with m is practically linear, while the variation of ω_{mn} with n is slightly nonlinear and the lowest frequency always occurs for $m = 1$ and $n = 0$.

The influence of the two geometric parameters, namely the stretching ratio $\delta = R_f/R_e$ and the normalized internal radius, $\delta_o = R_o/R_e$, is illustrated in Figs. 5 and 6. The linear frequencies are independent of the initial membrane thickness h. For the unstretched membrane ($\delta = 1$), $\omega_{mn} = 0$. As shown in Fig. 5 for the three lowest natural frequencies and two values of δ_o, as δ increases from one, the frequency increases quickly from zero and approaches a constant upper bound given for each pair of wave-numbers (m,n) by Eq. (29). This upper bound value increases as m and n increases, in agreement with the results shown in Fig. 4. Fig. 6(a) shows that, for a fixed pair (m,n), this upper bound increases with the geometric parameter $\delta_o = R_o/R_e$ in a nonlinear manner, as illustrated in Fig. 6(b). For $\delta > 2$ the natural frequency is practically constant. The tree lowest vibration modes are illustrated in Fig. 7. The sequence of modes is independent of the geometric parameters $\delta_o = R_o/R_e$ and $\delta = R_f/R_e$.

4.2. Nonlinear free vibration analysis

An extensive parametric finite element analysis involving moderate to large amplitude vibrations under free and forced conditions has shown that the in-plane displacements u and v are negligible when compared with the transversal displacement w during nonlinear vibrations of the membrane even when moderate to large amplitudes are considered, as illustrated in Fig. 8 where the displacement field related to a large amplitude vibration is illustrated for a given time t together with a comparison of the

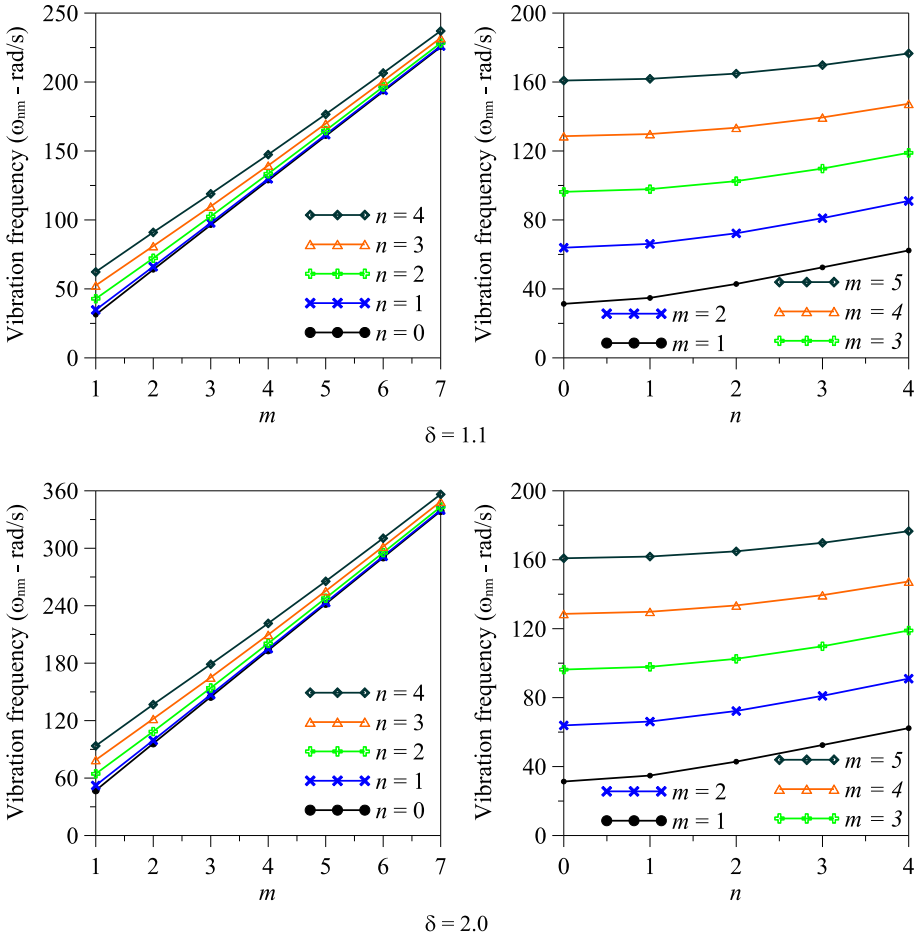

Fig. 4. Frequency spectrum (rad/s) for the annular membrane with $\delta_o = 0.20$.

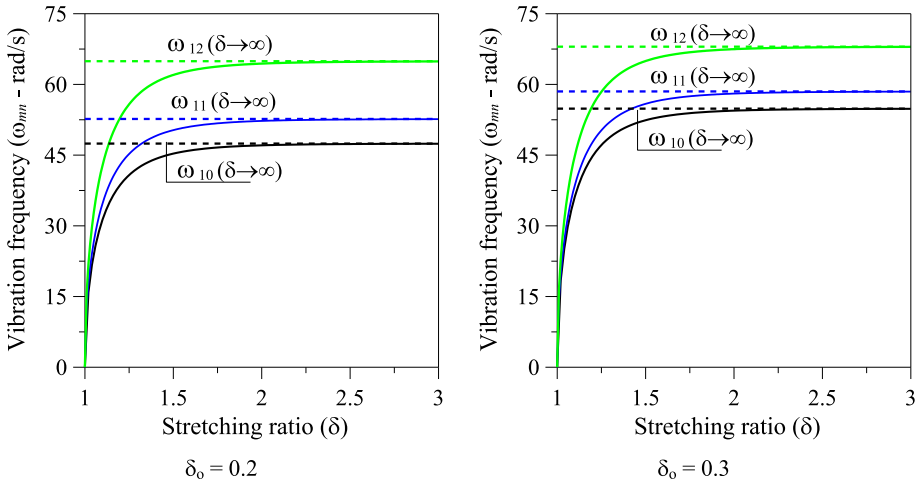

Fig. 5. Influence of the stretching ratio $\delta = R_f/R_e$ on the natural frequencies (rad/s).

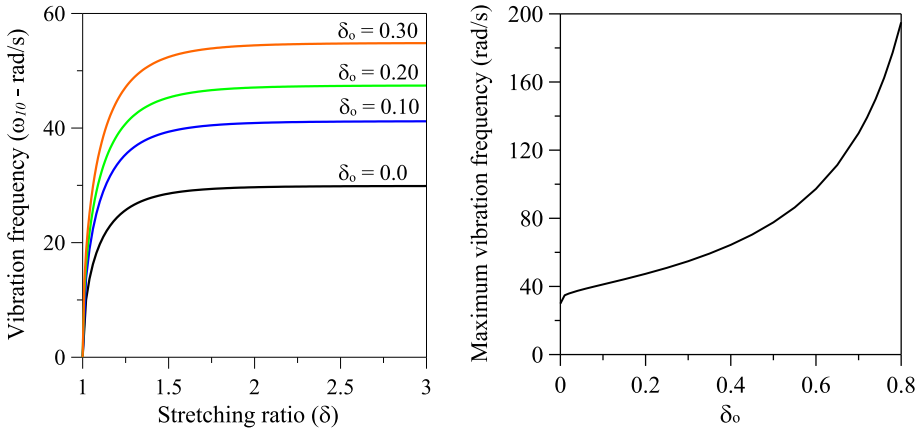

Fig. 6. Influence of the membrane geometric parameter $\delta_o = R_o/R_e$ on the natural frequencies (rad/s). ($m = 1$ and $n = 0$).

time response at point $(\rho,\theta) = (0.55,0)$ where the maximum displacements occur.

Thus, for the derivation of a low dimensional model for the nonlinear transversal vibrations of the membrane, the in-plane displacements u and v are neglected and Eq. (23.c) reduces to:

$$-\frac{\partial}{\partial\rho}\left(\rho\frac{\partial W}{\partial z_{,\rho}}\right)-\frac{\partial}{\partial\theta}\left(\rho\frac{\partial W}{\partial z_{,\theta}}\right)+\rho\Gamma\frac{\partial^2 w}{\partial t^2}=0 \tag{30}$$

The accuracy of this hypothesis is corroborated in the following analysis by comparing the present results with those obtained by the FEM where in-plane displacements and inertia forces are considered.

To obtain the nonlinear response of the stretched membrane, the transversal displacement field is approximated by a sum of *MxN* natural modes:

$$w(\rho,\theta,t)=\sum_{m=1}^{M}\sum_{n=0}^{N}A_{mn}(t)\left[CJ_n\left(\frac{\Lambda_{mn}\rho}{R_e}\right)-Y_n\left(\frac{\Lambda_{mn}\rho}{R_e}\right)\right]\cos(n\theta) \tag{31}$$

where $A_{mn}(t)$ are the time-dependent modal amplitudes and the Galerkin method is applied so that the nonlinear partial differential equation of motion in the transversal direction, Eq. (30), is transformed into a system of *MxN* ordinary differential equations of motion in the time domain. These equations are solved by numerical integration and using continuation techniques (Allgower and Georg, 1990).

The expansion of Eq. (30) in Taylor series leads to a nonlinear differential equation with only odd non-linear terms. By applying a perturbation procedure to this equation, as described in Gonçalves et al. (2008b), and assuming as seed mode the linear vibration mode, a modal expansion similar to (31) is obtained, thus justifying the choice of (31) as a valid approximation for the nonlinear displacement field.

Fig. 9 shows for $m = 1$ and $n = 0$ the variation of each modal amplitude in Eq. (31) considering an increasing number of terms in the Galerkin approximation ($N = 0$ and $M = 1,2,3$) for a stretched membrane with $\delta = 1.10$. The equations of motion are solved using continuation techniques, and the frequency-amplitude relation is obtained. The amplitudes A_{20} and A_{30} are rather small when compared to A_{10}. These results indicate that a reduced model with three degrees of freedom can describe with high precision the large amplitude vibrations of the membrane and reliable results can be obtained even when a one degree of freedom model ($M = 1$) is considered.

To evaluate the accuracy of the reduced order models, the amplitude-frequency relation is obtained using the finite element software Abaqus®. To do this, a mesh of 576 shell elements S4R, which is able to handle both the geometric and material nonlinearities, is used, and the response is obtained for a node on the undeformed membrane with the coordinates $(\rho,\theta) = (0.5,0)$. A total of

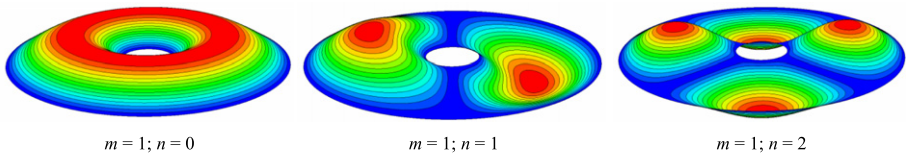

Fig. 7. Vibration modes of the annular membrane ($\delta_o = 0.20$).

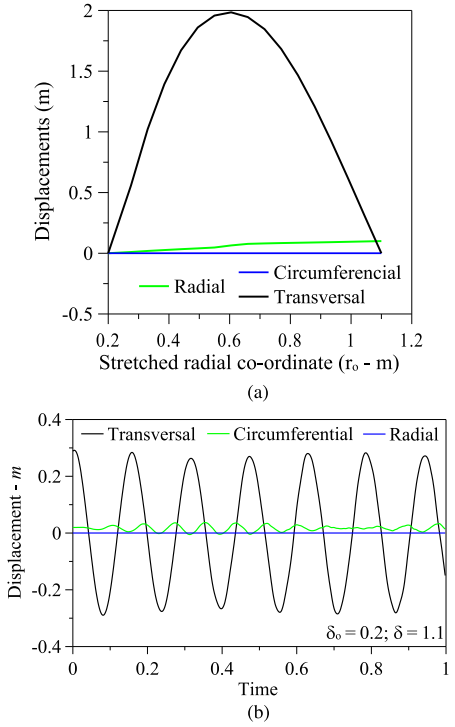

Fig. 8. (a) Variation of the in-plane radial and circumferential displacements and of the transversal displacement of the pre-stretched membrane for a given time t ($m = 1, n = 0$) during its free vibration response along the radial direction. (b) Time response of the three displacements at point $(\rho, \theta) = (0.55, 0)$. $\delta_o = 0.2$; $\delta = 1.1$.

1731 nonlinear equations of motion are numerically integrated, and the frequency-amplitude relation is obtained using the methodology proposed by Nandakumar and Chatterjee (2005), as follows: an initial displacement field in the form of the first nonlinear mode for a given amplitude is adopted and the time response of the lightly damped system is obtained for the chosen node, and the maximum amplitude and corresponding period between two consecutive positive peaks are computed at each cycle. Consider two successive peaks at times T_1 and T_2. Let their average value be A_1. Let the trough between these two positive peaks be A_2. The nonlinear frequency and corresponding amplitude are defined, respectively, as $\omega = 1/(T_1 - T_2)$ and $A = (A_1 - A_2)/2$. The finite element formulation naturally takes into account the influence of the in-plane displacements and inertia forces, which are neglected in the theoretical model. The FE results are compared with the results of the reduced order models obtained for the same set of coordinates in Fig. 10. An excellent agreement between the two models is observed up to very large deflections, corroborating the accuracy of the present model. For small vibration amplitudes, the response shows a strong increase in the natural frequency. As the vibration amplitude increases, the hardening effect decreases, and the curve veers upward tending to a constant frequency value for large vibration amplitudes. For a lightly stretched membrane a high degree of nonlinearity is expected with a strong increase of the vibration frequency with the vibration amplitude.

Fig. 11 shows the influence of the initial stretching ratio δ on the nonlinear frequency-amplitude relation. For any membrane geometry, as δ increases, the nonlinearity of the backbone curve decreases and approaches a linear behavior for $\delta > 2$. So, for a membrane under large radial strains, the nonlinear problem can be reduced to a linear one. All curves converge asymptotically to the same value of ω as the vibration amplitude increases. Both the natural frequency and the frequency-amplitude relation converge to same value of ω as δ increases (compare with results in Fig. 5). This value is given by Eq. (29). All frequencies depict the same nonlinear behavior observed here for $m = 1$ and $n = 0$.

The influence of the normalized internal radius δ_o is illustrated in Fig. 12. The nonlinearity increases as the internal radius approaches the external radius ($\delta_o = R_o/R_e \to 1$). For each geometry, a specific upper bound for the nonlinear frequency is obtained.

4.3. Forced nonlinear response

In the following the forced nonlinear vibrations of the annular membrane under a spatially uniform harmonic pressure is analyzed. The results of the axisymmetric vibrations of the membrane are shown in Figs. 13–19.

The nonlinear resonance curves for increasing values of the stretching ratio δ and $\delta_o = 0.20$ are shown in Fig. 13(a) where the transversal displacement of the steady-state response at

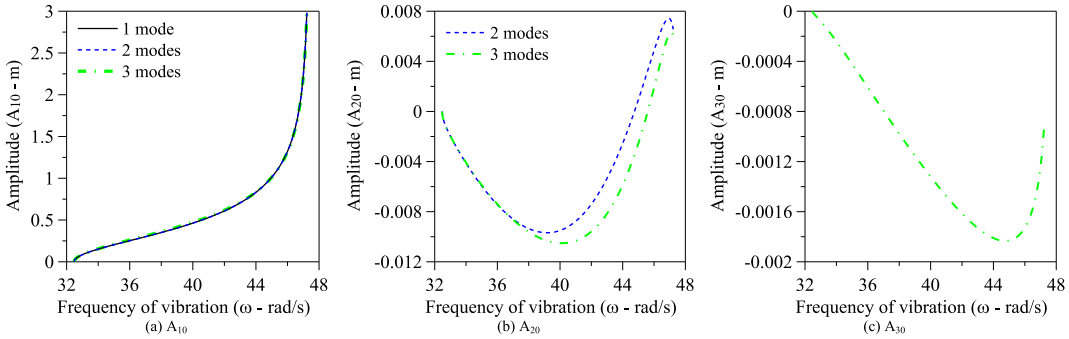

Fig. 9. Variation of the modal amplitudes A_i as a function of the frequency (rad/s), considering an increasing number of modes in Eq. (31). (a) A_{10}; (b) A_{20}; (c) A_{30} ($\delta = 1.10, \delta_o = 0.20$).

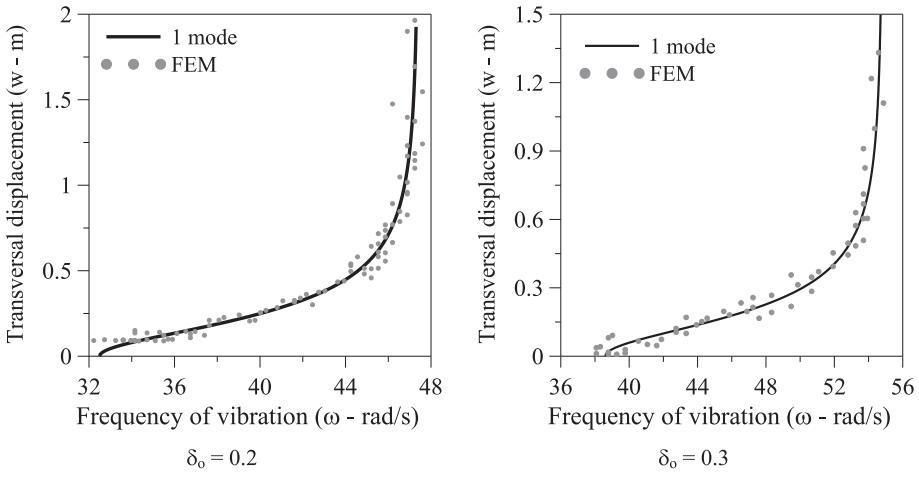

Fig. 10. Frequency-amplitude relation ($\delta = 1.10$). Transversal displacement w at a point $(\rho,\theta) = (0.5,0)$.

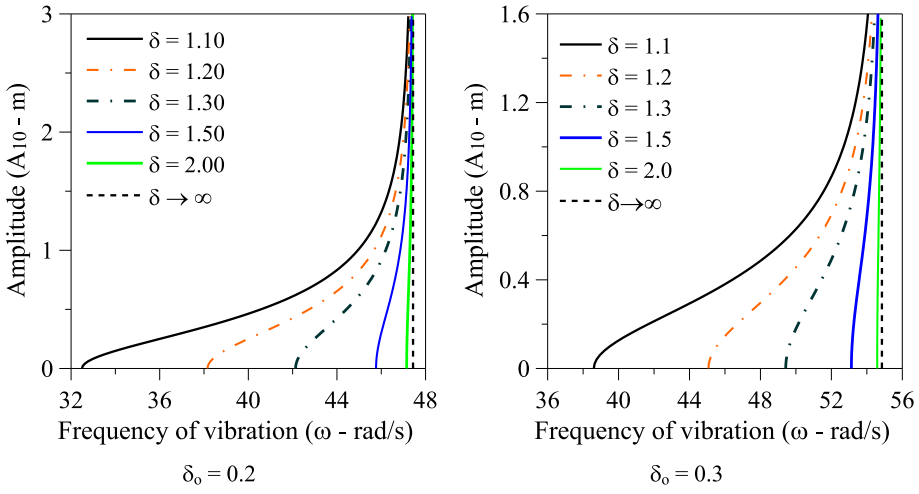

Fig. 11. Influence of the stretching ratio δ on the frequency-amplitude relation ($m = 1, n = 0$).

$(\rho,\theta) = (0.5,0)$ is plotted as a function of the forcing frequency. All curves converge to the linear resonance curve as the vibration amplitude increases. As δ increases, the nonlinearity decreases, and the response is nearly linear for $\delta = 2.0$ and higher. The influence of the internal radius is shown in Fig. 13(b). The nonlinearity increases as the inner radius increases and approaches the outer boundary ($\delta_o = R_o/R_e \to 1$), particularly in the initial stage of the response.

The bifurcation diagrams of the Poincaré map, obtained by continuation techniques, for three selected values of the stretching ratio δ, $P_o = 1$ and $\delta_o = 0.20$, is shown in Fig. 14 where the co-ordinate A_{10} is plotted as a function of the forcing frequency Ω. Fig. 15 shows, for selected values of the excitation frequency and δ, the bifurcation diagrams as a function of the forcing magnitude P_o. Here and henceforth, dashed lines represent unstable responses, while continuous lines represent stable responses. The stable and unstable branches are separated by saddle-node bifurcations (SN), as usually happens in nonlinear resonance curves. Depending on the value of P_o and Ω, the membrane may display either one or three coexisting responses, two stable and one unstable. So, under a continuously varying dynamic loading the membrane may display sudden changes in phase and vibration amplitudes due to these dynamic bifurcations. Also, in some investigations considerable increase in frequency is sometimes observed with vibration amplitudes as in the present analysis (Decraemer et al., 1989; Recio et al., 1998).

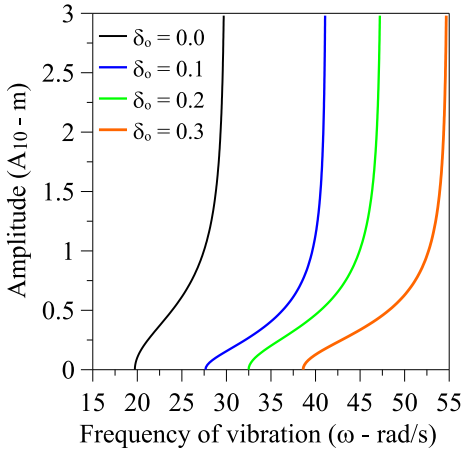

Fig. 12. Influence of the inner radius ($\delta_o = R_o/R_e$) on the frequency-amplitude relation ($\delta = 1.10, m = 1, n = 0$).

Fig. 16 presents bifurcation diagrams as a function of the excitation magnitude for increasing values of the damping

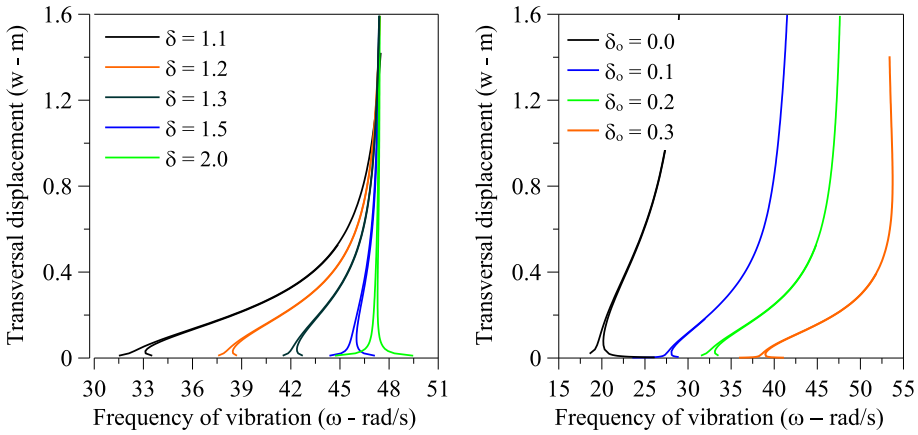

Fig. 13. Nonlinear resonance curves for (a) increasing values of the stretching ratio δ and $\delta_o = 0.20$ and (b) increasing values of the internal radius ratio δ_o and $\delta = 1.1$.

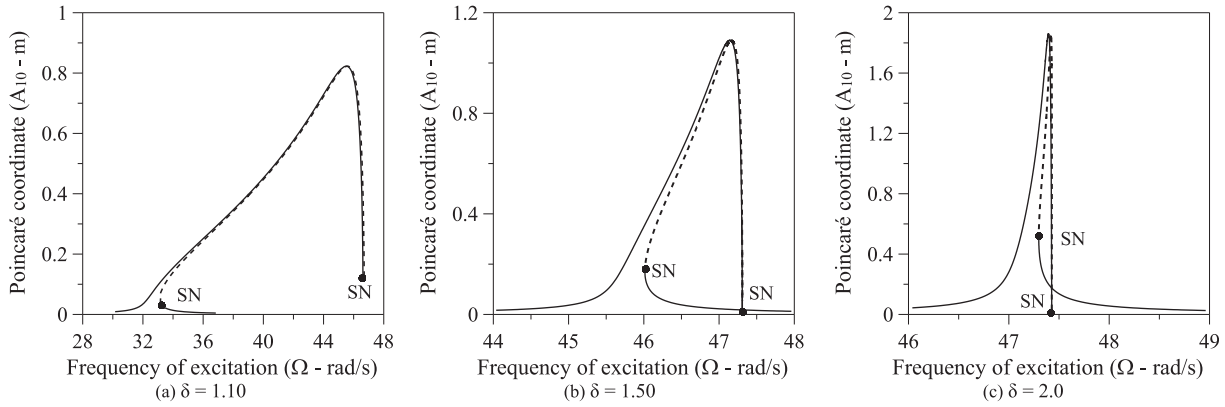

Fig. 14. Bifurcation diagrams for increasing pre-stretching ratios. Coordinate A_{10} as a function of the excitation frequency Ω (P_o=1; c = 0.05). (a) $\delta = 1.10$; (b) $\delta = 1.50$; (c) $\delta = 2.0$.

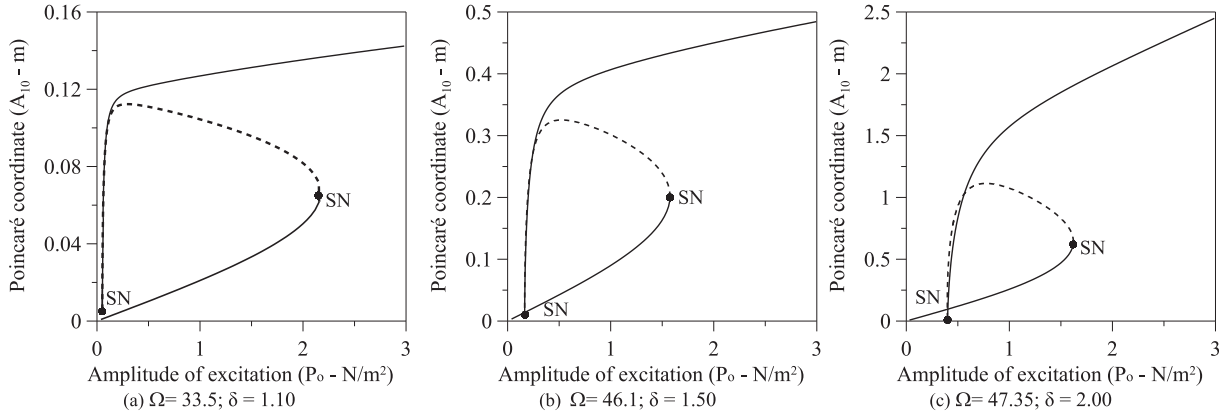

Fig. 15. Bifurcation diagrams for selected values of the excitation frequency, Ω and stretching ratio δ. Co-ordinate A_{10} as a function of the forcing amplitude P_o. c = 0.05. (a) $\Omega = 33.5$; $\delta = 1.10$; (b) $\Omega = 46.1$; $\delta = 1.50$; (c) $\Omega = 47.35$; $\delta = 2.00$.

parameter c. For $\delta = 1.1$ and $\Omega = 33.5$, Fig. 16(a), the range where three coexisting solutions appears decreases as the damping parameter increases and disappears at $c = 3$. As δ increases, the region where multi-stability exists decreases, as shown in Fig. 16(b) for $\delta = 2.0$ and $\Omega = 47.35$. The variation of the load coordinates of the two saddle points with the damping parameter c for $\delta = 1.1$ and $\Omega = 33.5$ is show in Fig. 17, illustrating the decreasing range where unstable solutions occur. The same decrease in complexity occurs as the forcing frequency departs from the resonance region. The results in Fig. 18 illustrate the influence of the damping on the resonance curves.

The influence of the system and force parameters on the degree of nonlinearity of the membrane response can also be observed in the topological complexity of the basins of attraction. Fig. 19 illustrates the basins of attraction of the membrane for three sets of parameters and $c = 0.05$, $\delta_o = 0.2$ and $P_o = 1$: (a) $\delta = 1.1$; $\Omega = 33.5$; (b) $\delta = 1.5$; $\Omega = 46.1$ and (c) $\delta = 2.0$; $\Omega = 47.35$. The dark grey area is the basin of attraction of the resonant large amplitude oscillation, while the light grey area corresponds to the basin of attraction of the small amplitude oscillation. The black crosses in each figure are fixed point of the Poincaré Map (attractor) of each stable solution. The size of the continuous basin of attraction can be used as a

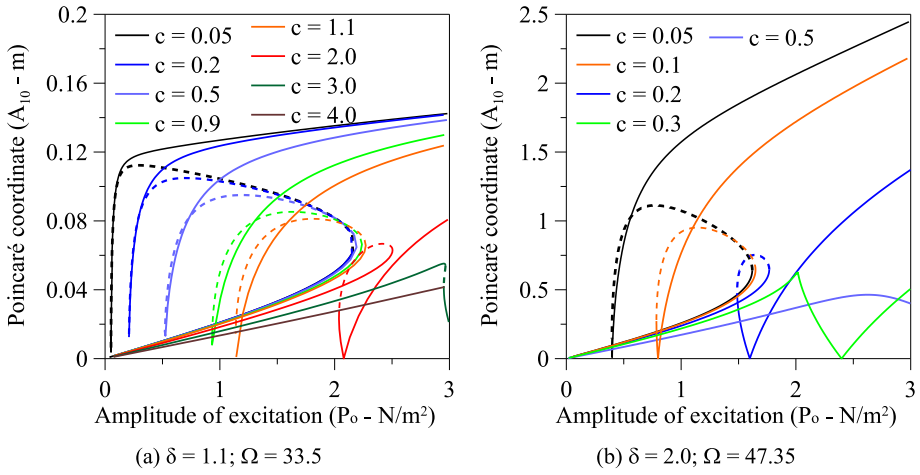

Fig. 16. Influence on the damping coefficient c on the non-linear behavior and stability of the membrane. $P_o = 1$.

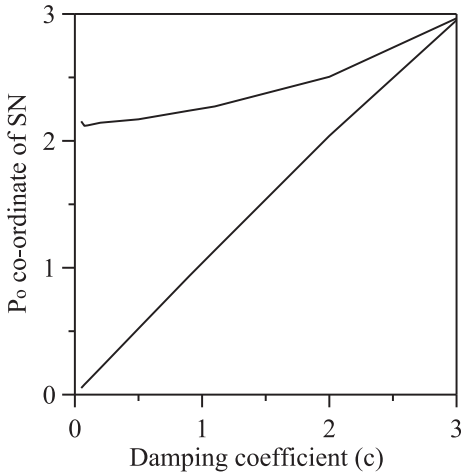

Fig. 17. Influence of the damping on the saddles.

measure of the integrity and robustness of a dynamic solution under external perturbations or uncertainties in the systems parameters as shown in Gonçalves and Santee (2008a) and Gonçalves et al. (2011). So, neighboring initial conditions far from the attractors may lead to different steady-state solutions and complex transients due to the topological complexity of the basins in this region. It is interesting to notice that most initial conditions lead to the large amplitude resonant response.

5. Conclusions

The mathematical modeling for the nonlinear vibration analysis of a radially pre-stretched hyperelastic annular membrane under finite deformations was presented. Alternative solutions for the static and dynamic analysis were presented and compared with the results obtained by the finite element method. The static solution is a function of the material constant, the stretching ratio in the radial direction (deformed outer radius/ undeformed outer radius) and the ratio of the inner to the outer radius. The natural frequency associated with each vibration mode increases from zero as the initial radial stretch increases and approaches an upper bound, being practically constant for a stretching ratio equal or higher then two. This upper bound increases as the ratio of the inner to the outer radius increases and approaches the physical limit of one. The results show that, for the nonlinear vibration analysis, a single degree-of-freedom model can give accurate results up to very large deflections. The accuracy of this low order model is verified via comparisons with the higher order modal approximations, and the numerical values computed by the finite element method, which compare well with the theoretical results up to very large deflections. The results highlight the influence of the stretching ratio and annular membrane geometry on the nonlinear frequency-amplitude relation, and bifurcation diagrams. It is shown that a lightly stretched membrane displays a highly nonlinear hardening response, that the nonlinearity decreases as the stretching ratio increases, and the response becomes practically linear for a deformed radius of twice the initial value or higher. Both the frequency-amplitude relation and the corresponding linear frequency

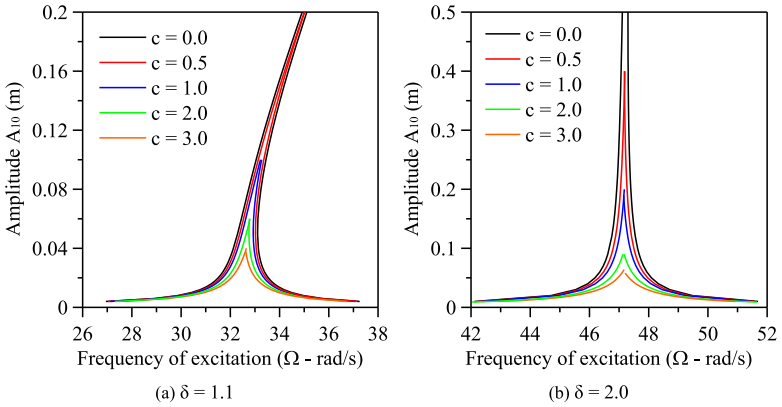

Fig. 18. Influence on the damping coefficient c on the non-linear resonance curves of the membrane. $P_o = 1$.

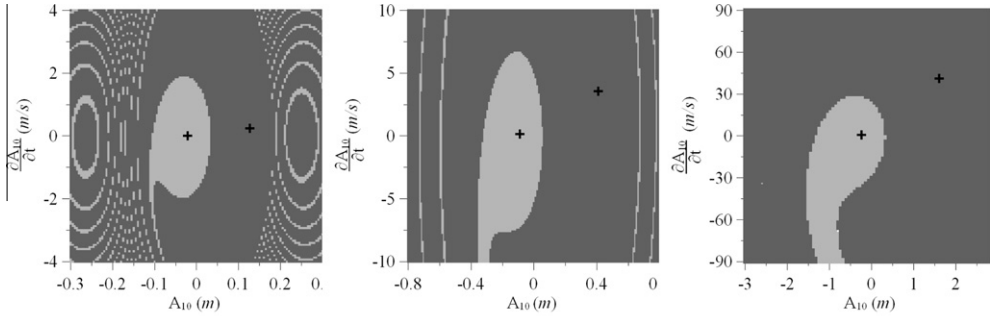

Fig. 19. Basins of attraction for selected values of the control parameters. ($c = 0.05$; $\delta_o = 0.2$; $P_o = 1$). (a) $\delta = 1.1$; $\Omega = 33.5$; (b) $\delta = 1.5$; $\Omega = 46.1$; (c) $\delta = 2.0$; $\Omega = 47.35$. Dark grey: basin of attraction of the resonant large amplitude oscillation. Light grey: Basin of attraction of the small amplitude oscillation. Black cross: fixed point of the Poincaré map (attractor).

converge to the same frequency upper bound as the radial stretch and/or vibration amplitude increases. This explains the accuracy of the low order models for large finite amplitude oscillations of the hyperelastic membrane. In the main resonance region multiplicity of solutions is observed due to both material and geometric nonlinearities. This may lead to sudden jumps in vibration amplitude and complex transients which are a function of the load control parameters and damping. The complexity of the nonlinear oscillations in this region is illustrated by several bifurcations diagrams and basins of attraction. The present methodology for the nonlinear dynamic analysis of hyperelastic membranes and for the derivation of reduced order models can be applied to other membrane geometries and constitutive laws, leading to a better understanding of the dynamics of this class of structures and to new technological applications of thin membranes.

Acknowledgments

The authors acknowledge the financial support of the Brazilian Research Agencies CAPES, CNPq and FAPERJ.

Appendix A

Coefficients $L_i(\rho)$ in Eq. (25) derived from Eq. (18):

$$L_1 = \frac{-\rho^2}{\left(A_1/\rho + 2A_2\rho\log\rho + A_2\rho + 2A_3\rho + A_4\right)^4} \times \frac{1}{\left(A_1\log\rho + A_2\rho^2\log\rho + A_3\rho^2 + A_4\rho + A_5\right)^2} \tag{32.a}$$

$$\begin{aligned} L_2 = &-\frac{4\rho^2}{\left(A_1/\rho + 2A_2\rho\log\rho + A_2\rho + 2A_3\rho + A_4\right)^5} \times \frac{\left(-A/\rho^2 + 2B\log\rho + 3B + 2C\right)}{\left(A_1\log\rho + A_2\rho^2\log\rho + A_3\rho^2 + A_4\rho + A_5\right)^2} \\ &+ -\frac{3\rho}{\left(A_1/\rho + 2A_2\rho\log\rho + A_2\rho + 2A_3\rho + A_4\right)^4} \times \frac{1}{\left(A_1\log\rho + A_2\rho^2\log\rho + A_3\rho^2 + A_4\rho + A_5\right)^2} \\ &+ \frac{2\rho^2}{\left(A_1/\rho + 2A_2\rho\log\rho + A_2\rho + 2A_3\rho + A_4\right)^3} \times \frac{1}{\left(A_1\log\rho + A_2\rho^2\log\rho + A_3\rho^2 + A_4\rho + A_5\right)^3} \end{aligned} \tag{32.b}$$

$$L_3 = \frac{-\rho^2}{\left(A_1/\rho + 2A_2\rho\log\rho + A_2\rho + 2A_3\rho + A_4\right)^2} \times \frac{1}{\left(A_1\log\rho + A_2\rho^2\log\rho + A_3\rho^2 + A_4\rho + A_5\right)^4} \tag{32.c}$$

Appendix B

Coefficients $L_i(\rho)$ in Eq. (25) derived from Eq. (21):

$$L_1 = \frac{-\rho^{12}\left(R_e^2 - R_o^2\right)^6}{\left(\left(R_fR_e - R_o^2\right)\rho^2 + R_o^2\left(R_fR_e - R_e^2\right)\right)^4\left(\left(R_fR_e - R_o^2\right)\rho^2 - R_o^2\left(R_fR_e - R_e^2\right)\right)^2} \tag{33.a}$$

$$\begin{aligned} L_2 = &\frac{-3\rho^{11}\left(R_e^2 - R_o^2\right)^6}{\left(\left(R_fR_e - R_o^2\right)\rho^2 + R_o^2\left(R_fR_e - R_e^2\right)\right)^4\left(\left(R_fR_e - R_o^2\right)\rho^2 - R_o^2\left(R_fR_e - R_e^2\right)\right)^2} \\ &- \frac{8\rho^{11}\left(R_e^2 - R_o^2\right)^6R_o^2\left(R_fR_e - R_e^2\right)}{\left(\left(R_fR_e - R_o^2\right)\rho^2 + R_o^2\left(R_fR_e - R_e^2\right)\right)^5\left(\left(R_fR_e - R_o^2\right)\rho^2 - R_o^2\left(R_fR_e - R_e^2\right)\right)^2} \\ &+ \frac{2\rho^{11}\left(R_e^2 - R_o^2\right)^6}{\left(\left(R_fR_e - R_o^2\right)\rho^2 + R_o^2\left(R_fR_e - R_e^2\right)\right)^3\left(\left(R_fR_e - R_o^2\right)\rho^2 - R_o^2\left(R_fR_e - R_e^2\right)\right)^3} \end{aligned} \tag{33.b}$$

$$L_3 = \frac{-\rho^{10}\left(R_e^2 - R_o^2\right)^6}{\left(\left(R_fR_e - R_o^2\right)\rho^2 + R_o^2\left(R_fR_e - R_e^2\right)\right)^2\left(\left(R_fR_e - R_o^2\right)\rho^2 - R_o^2\left(R_fR_e - R_e^2\right)\right)^4} \tag{33.c}$$

References

Abaqus version 6.5 Standard User's Manual, 2001. Hibbitt, Karlsson, and Sorensen Inc., Pawtucket, USA.

Allgower, E., Georg, K., 1990. An Introduction, Numerical Continuation Methods. Springer-Verlag, Berlin.

Asmar, N.H., 2005. Partial Differential Equations with Fourier series and Boundary Value Problems. Pearson Prentice Hall, Upper Saddle River.

Bala Subrahmanyam, P., Sujith, R.I., 2001. Exact solutions for axisymmetric vibrations of solid circular and annular membranes with continuously varying density. Journal of Sound and Vibration 248, 371–378.

Balestrini, J.L., Skorinko, J.K., Hera, A., Gaudette, G.R., Billiar, K.L., 2010. Applying controlled non-uniform deformation for in vitro studies of cell mechanobiology. Biomech Model Mechanobiology 9, 329–344.

Buchanan, G.R., 2005. Vibration of circular membrane with linearly varying density along a diameter. Journal of Sound and Vibration 280, 407–414.

Chakravarty, U.K., Albertani, R., 2010. Experimental and finite element modal analysis of a pliant membrane for micro air vehicles wings. In: 51st AIAA/ASME/ASCE/AHS/ASC Structures, Structural Dynamics and Materials Conference, pp. 2010–2710.

Chang-Jiang, L., Zhou-Lian, Z., Xiao-Ting, H., Jun-Yi, S., Wei-Ju, S., Yun-Ping, X., Jun, L., 2010. L-P perturbation solution of nonlinear free vibration of prestressed orthotropic membrane in large amplitude. Mathematical Problems in Engineering 2010, art. no. 561364.

Chou-Wang, M.S., Horgan, C.O., 1989. Cavitation in nonlinear elastodynamics for neo-Hookean materials. International Journal of Engineering Science 27, 967–973.

David, F.G., 2005. Mechanics of nonlinear biomembranes: application to ophthalmology. Texas A& M University, Ph.D thesis

David, G., Humphrey, J.D., 2004. Redistribution of stress due to a circular hole in a nonlinear anisotropic membrane. Journal of Biomechanics 37, 1197–1203.

Decraemer, W.F., Khanna, S.M., Funnell, W.R., 1989. Interferometric measurement of the amplitude and phase of tympanic membrane vibrations in cat. Hearing Research 38, 1–17.

Foster, H.O., 1967b. Very large deformations of axially symmetrical membranes made of neo-Hookean materials. International Journal of Engineering Science 5, 95–117.

Fox, J.W., Goulbourne, N.C., 2008. On the dynamic electromechanical loading of dielectric elastomer membranes. Journal of the Mechanics and Physics of Solids 56, 2669–2686.

Fox, J.W., Goulbourne, N.C., 2009. Electric field-induced surface transformations and experimental dynamic characteristics of dielectric elastomer membranes. Journal of the Mechanics and Physics of Solids 57, 1417–1435.

Fu, Y.B., Ogden, R.W., 2001. Nonlinear Elasticity – Theory and Applications. Lecture Notes Series, vol. 283. Cambridge University Press, Cambridge.

Fulton, J.P., Simmonds, J.G., 1986. Large deformations under vertical edge loads of annular membranes with various strain energy densities. International Journal of Nonlinear Mechanics 21, 257–267.

Gonçalves, P.B., Santee, D., 2008a. Influence of uncertainties on the dynamic buckling loads of structures liable to asymmetric post-buckling behavior. Mathematical Problems in Engineering, 24. Article ID 490137.

Gonçalves, P.B., Silva, F.M.A., Del Prado, Z.J.G.N., 2008b. Low dimensional models for the nonlinear vibration analysis of cylindrical shells based on a perturbation procedure and proper orthogonal decomposition. Journal of Sound and Vibration 315, 641–663.

Gonçalves, P.B., Soares, R.M., Pamplona, D., 2009. Nonlinear vibrations of a radially stretched circular hyperelastic membrane. Journal of Sound and Vibration 327, 231–248.

Gonçalves, P.B., Silva, F.M.A., Rega, G., Lenci, S., 2011. Global dynamics and integrity of a two-dof model of a parametrically excited cylindrical shell. Nonlinear Dynamics 63, 61–82.

Goulbourne, N., Frecker, M., Mockensturm, E., 2004. Electro-elastic modeling of a dielectric elastomer diaphragm for a prosthetic blood pump, In: Proceedings of SPIE, Smart Structures and Materials on Electroactive Polymers and Devices, pp. 122–133.

Goulbourne, N.C., Mockensturm, E.M., Frecker, M., 2005. A nonlinear model for dielectric elastomer membranes. ASME Journal of Applied Mechanics 72, 899–906.

Grabmüller, H., Novak, E., 1987. Nonlinear boundary value problems for the annular membrane: a note on uniqueness of positive solutions. Journal of Elasticity 17, 279–284.

Green, A.E., Adkins, J.E., 1960. Large Elastic Deformations and Nonlinear Continuum Mechanics. Oxford University Press, Oxford.

Gutierrez, R.H., Laura, P.A.A., Bambill, D.V., Jederlinic, V.A., Hodges, D.H., 1998. Axisymmetric vibrations of solid circular and annular membranes with continuously varying density. Journal of Sound and Vibration 212, 611–622.

Hite, W.J.III., Peddieson, J., 1977. Finite deflections of annular membranes. Industrial Mathematics 27, 75–86.

Jabareen, M., Eisenberger, M., 2001. Free vibrations of non-homogeneous circular and annular membranes. Journal of Sound and Vibration 240, 409–429.

Jenkins, C.H., Korde, U.A., 2006. Membrane vibration experiments: an historical review and recent results. Journal of Sound and Vibration 295, 602–613.

Jenkins, C.H., Leonard, J.W., 1991. Nonlinear dynamic response of membranes: state of the art. ASME Applied Mechanics Reviews 44, 319–328.

Jiang, L., 1996. Application of the Taylor–Galerkin finite element and Godunov-type finite difference methods to finite amplitude axisymmetric waves in hyperelastic membranes. Journal of Sound and Vibration 192, 223–244.

Laura, P.A.A., Rossit, C.A., La Malfa, S., 1998. Transverse vibrations of composite, circular annular membranes: exact solution. Journal of Sound and Vibration 212, 611–622.

Lavergne, T., Durand, S., Bruneau, M., Joly, N., Rodrigues, D., 2010. Dynamic behavior of the circular membrane of an electrostatic microphone: effect of holes in the backing electrode. Journal of the Acoustical Society of America 128, 3459–3477.

Libai, A., Simmonds, J.G., 1998. The Nonlinear Theory of Elastic Shells, second ed. Cambridge University Press, Cambridge.

Lladó, A., Guimerá, J., Garcia, F., Navarro, A., 1999. Expanded polytetrafluoroethylene membrane for the prevention of peridural fibrosis after spinal surgery: an experimental study. Eur Spine Journal 8, 138–143.

Na, T.Y., Kurajian, G.M., 1976. General solution of the problem of large deflection of an annular membrane under pressure. Aeronautical Quarterly 27, 195–200.

Nandakumar, K., Chatterjee, A., 2005. Resonance, parameter estimation, and modal interections in a strongly nonlinear benchtop oscillator. Nonlinear Dynamics 40, 149–167.

Nayfeh, A.H., Balashandran, B., 1995. Applied Nonlinear Dynamics. John Wiley & Sons, New York.

Noga, S., 2010. Free transverse vibration analysis of an elastically connected annular and circular double-membrane compound system. Journal of Sound and Vibration 329, 1507–1522.

Pamplona, D.C., Bevilacqua, L., 1992. Large deformations under axial force and moment loads of initially flat annular membranes. International Journal of Nonlinear Mechanics 27, 639–650.

Pelrine, R., Kornbluh, R., Pei, Q., Joseph, J., 2000. High-speed electrically actuated elastomers with strain greater than 100%. Science 287, 836–839.

Pinto, F., 2006. Analytical and experimental investigation on a vibrating annular membrane attached to a central free, rigid core. Journal of Sound and Vibration 291, 1278–1287.

Prendergast, P.J., Kelly, D.J., Rafferty, M., Blayney, A.W., 1999. The effect of ventilation tubes on stresses and vibration motion in the tympanic membrane: a finite element analysis. Clinical Otolaryngology & Allied Sciences 24, 542–548.

Recio, A., Rich, N.C., Narayan, S.S., Ruggero, M.A., 1998. Basilar-membrane responses to clicks at the base of the chinchilla cochlea. Journal of the Acoustical Society of America 103, 1972–1989.

Rega, G., Troger, H., 2005. Dimension reduction of dynamical systems: Methods, models, applications. Nonlinear Dynamics 41, 1–15.

Rivlin, R.S., 1948a. Large elastic deformations of isotropic materials. Philosophical Transactions of the Royal Society A 240, 459–491.

Rivlin, R.S., 1948b. Large elastic deformations of isotropic materials: I. Fundamental concepts. II. Some uniqueness theorems for pure homogeneous deformation. Philosophical Transactions of the Royal Society of London A240, 459–508.

Rossing, T.D., 2000. Science of Percussion Instruments. World Scientific Publications Co Inc, New York.

Roxburgh, D.G., Steigmann, D.J., Tait, R.J., 1995. Azimuthal shearing and transverse deflection of an annular elastic membrane. International Journal of Engineering and Science 33, 27–43.

Saccomandi, G., Ogden, R.W., 2004. Mechanics and Thermomechanics of Rubber like Solids. Springer, Wien, CISM Courses and Lectures No.452.

Saravanan, U., 2011. On large elastic deformation of prestressed right circular annular cylinders. International Journal of Nonlinear Mechanics 46, 96–113.

Selvadurai, A.P.S., 2006. Deflections of a rubber membrane. Journal of the Mechanics and Physics of Solids 54, 1093–1119.

Soares, R.M., 2009. Dynamic Analysis of Circular Hyperelastic Membranes, Doctoral Thesis, Pontifical Catholic University of Rio de Janeiro, Rio de Janeiro, Brazil.

Tezduyar, T.E., Wheeler, L.T., Graux, L., 1987. Finite deformation of a circular elastic membrane containing a concentric rigid inclusion. International Journal of Nonlinear Mechanics 22, 61–72.

Tielking, J.T., Feng, W.W., 1974. The application of the minimum potential energy principle to nonlinear axisymmetric membrane problems. Journal of Applied Mechanics 41, 491–496.

Tobis, J., Tintut, Y., Mal, A.K., Klug, W.S., Demer, L.L., Hoshino, T., Chow, L.A., Hsu, J.J., Perlowski, A.A., Abedin, M., 2009. Mechanical stress analysis of a rigid inclusion in distensible material: a model of atherosclerotic calcification and plaque vulnerability. American Journal of Physiology-heart and Circulatory Physiology 297, H802–H810.

Treloar, L.R.G., 1975. Physics of Rubber Elasticity, third ed. University Press, Oxford.

Volandri, G., DiPuccio, F., Forte, P., Carmignani, C., 2011. Biomechanics of the tympanic membrane. Journal of Biomechanics 44, 1219–1236.

Wang, C.Y., 2003. Vibration of an annular membrane attached to a free, rigid core. Journal of Sound and Vibration 260, 776–782.

Wang, M., Steigmann, D.J., 1997. Small oscillations of finitely deformed elastic networks. Journal of Sound and Vibration 202, 619–631.

Willatzen, M., 2002. Exact power series solutions for axisymmetric vibrations of circular and annular membranes with continuously varying density in the general case. Journal of Sound and Vibration 258, 981–986.

Wineman, A., 2005. Some results for generalized neo-Hookean elastic materials. International Journal of Nonlinear Mechanics 40, 271–279.

Wong, F.S., Shield, R.T., 1969. Large plane deformations of thin elastic sheets of neo-Hookean material. Journal of Applied Mathematics and Physics 20, 176–199.

Zhu, J., Cai, S., Suo, Z., 2010. Resonant behavior of a membrane of a dielectric elastomer. International Journal of Solids and Structures 47, 3254–3262.